Production of functional small interfering RNAs by an amino-terminal deletion mutant of human Dicer

Edward M. Kennedy, Adam W. Whisnant, Anand V. R. Kornepati, Joy B. Marshall, Hal P. Bogerd, and Bryan R. Cullen[1]

Department of Molecular Genetics & Microbiology, Center for Virology, Duke University Medical Center, Durham, NC 27710

Although RNA interference (RNAi) functions as a potent antiviral innate-immune response in plants and invertebrates, mammalian somatic cells appear incapable of mounting an RNAi response and few, if any, small interfering RNAs (siRNAs) can be detected. To examine why siRNA production is inefficient, we have generated double-knockout human cells lacking both Dicer and protein kinase RNA-activated. Using these cells, which tolerate double-stranded RNA expression, we show that a mutant form of human Dicer lacking the amino-terminal helicase domain can process double-stranded RNAs to produce high levels of siRNAs that are readily detectable by Northern blot, are loaded into RNA-induced silencing complexes, and can effectively and specifically inhibit the expression of cognate mRNAs. Remarkably, overexpression of this mutant Dicer, but not wild-type Dicer, also resulted in a partial inhibition of Influenza A virus—but not poliovirus—replication in human cells.

RNA interference | Dicer | microRNAs | innate immunity | small interfering RNAs

RNA interference (RNAi) is believed to have initially evolved as an innate immune response to viral infection that was then adapted to become a mechanism for the posttranscriptional regulation of cellular gene expression using genomically encoded microRNAs (miRNAs) (1, 2). Considerable evidence indicates that RNAi remains a key antiviral immune response in plants, nematodes, and insects. However, whether RNAi as originally defined—that is a posttranscriptional regulatory mechanism triggered by long double-stranded RNAs (dsRNAs) (3)—continues to function as an antiviral mechanism in mammalian cells has remained controversial. Most importantly, sequence analysis of small RNAs expressed in mammalian somatic cells infected by a wide range of viruses has failed to detect significant levels of virally derived siRNAs (4–7), whereas human and mouse cells lacking a functional Dicer protein, and hence incapable of producing either siRNAs or miRNAs, are generally very similar to WT cells in terms of their ability to support the replication of a wide range of RNA and DNA viruses (5, 6), thus arguing against the existence of a protective RNAi response.

Although the preponderance of evidence therefore indicates that mammalian somatic cells are unable to produce functionally significant levels of siRNAs, this does not appear to be true for mouse germ cells and embryonic stem (ES) cells, which can produce readily detectable and biologically active levels of siRNAs from long dsRNA substrates (8–12). This observation suggested that these undifferentiated murine cells might express an alternative isoform of Dicer that had acquired the ability to effectively cleave long dsRNAs. Indeed, Flemr et al. (13) subsequently reported that mouse oocytes express an amino-terminally truncated form of Dicer that arises from a novel mRNA transcribed from a retrotransposon-derived promoter present in intron 6 of the mouse Dicer (dcr) gene. This Dicer isoform, which lacks the amino-terminal 228 aa of full-length Dicer, was found to process ectopically expressed long dsRNA hairpins into siRNAs that could modestly but detectably down-regulate a cognate indicator construct (13). This result was consistent with earlier biochemical data showing that mild protease treatment of purified Dicer enhances dsRNA processing in vitro (14, 15), and more recent results arguing that the amino-terminal

helicase domain of Dicer attenuates the processing of long dsRNAs, whereas pre-miRNA processing is unaffected (16).

Although these data raise the possibility that RNAi might be active in specific mammalian cell populations, including germ cells and ES cells, the retrotransposon promoter that gives rise to the truncated Dicer seen in rodent germ cells is absent in humans and other primates (13), and it remains unclear whether the human dcr gene can also give rise to alternative isoforms that can process long dsRNAs into siRNAs. Here, we present data demonstrating that deletion of the N-terminal helicase domain of human Dicer (hDcr) indeed enhances its ability to process endogenously transcribed dsRNAs into biologically active siRNAs, and we further demonstrate that this mutated form of hDcr can give rise to viral siRNAs that are loaded into the host RNA-induced silencing complex (RISC) in infected cells.

Results

Mutants of Human Dicer Lacking the Helicase Domain Efficiently Process pre-miRNAs.

To test whether hDcr variants lacking all or part of the helicase domain can effectively generate mature miRNAs and siRNAs in human cells, we constructed three N-terminal deletion mutants of hDcr, called F1, N1, and N3. The F1 mutant is identical in structure to the murine Dicer isoform described by Flemr et al. (13), although this variant cannot naturally exist in human cells because of the absence of the MT-C retrotransposon found in intron 6 of mouse dcr. The F1 variant of hDcr lacks the first 228 aa of the helicase domain and instead contains a translation initiation codon and six additional N-terminal amino acids normally contributed by the murine MT-C retroelement. We considered that alternative isoforms of hDcr might arise as a result of translation

Significance

Although RNA interference (RNAi) is an important antiviral innate-immune response in plants and invertebrates, whether mammals mount effective RNAi responses remains controversial. Using human cells lacking functional Dicer and protein kinase RNA-activated genes, we examined whether wild-type or a deletion mutant of Dicer, lacking the helicase domain, could induce RNAi when presented with double-stranded RNAs derived from plasmids or generated during viral infections. Overexpression of the truncated Dicer mutant resulted in the production of siRNAs in both cases, and these were sufficient to inhibit the expression of cognate mRNAs. Whether the latent ability of human Dicer to induce RNAi will ever be unmasked in vivo remains unclear.

initiation at internal methionine codons and noted the presence of methionine codons at positions 496 and 606 in hDcr. The N1 hDcr mutant was therefore designed to initiate translation at position 496, whereas the N3 mutant was designed to initiate at position 606 (Fig. 1A). To confirm expression and function, we cotransfected the previously described (17) hDcr-deficient NoDice cell line, derived by inactivation of all three copies of the *dcr* gene in human 293T cells by DNA editing, with expression vectors encoding WT hDcr, or the F1, N1, or N3 mutants of hDcr, together with a plasmid expressing pri-miR-155, a pri-miRNA precursor that is not normally expressed by NoDice or 293T cells (Fig. S1A). As shown in Fig. 1B, we detected each of these proteins in transfected NoDice cells by Western blot analysis using a polyclonal anti-Dicer antiserum. As shown in Fig. 1C, we observed readily detectable levels of pre-miR-155, which arises by cleavage of pri-miR-155 by endogenous Drosha, in all transfected cell cultures. Expression of WT hDcr or of the N1 hDcr mutant gave rise to high levels of mature miR-155, whereas moderate levels of miR-155 were detected in the NoDice cells expressing the F1 mutant. In contrast, the N3 mutant of hDcr, which bears the most extensive deletion (Fig. 1A), gave rise to low levels of mature miR-155 (Fig. 1C).

To further investigate the ability of the N1 and F1 hDcr mutants to process pre-miRNAs appropriately, we also analyzed the expression of mature miRNAs of endogenous origin by small RNA-seq (Fig. 1 D–G) or by quantitative RT-PCR (qRT-PCR) (Fig. S1B). As shown in Fig. 1D, deep sequencing confirmed the almost complete absence of mature miRNAs in the parental NoDice cells (17) but showed that expression of endogenous mature miRNAs

was rescued by transfection with a vector expressing WT hDcr. Comparison of NoDice cells transiently expressing full-length hDcr or the N1 mutant revealed that these two proteins gave rise to essentially identical patterns of mature miRNA expression (Fig. 1E). In contrast, the F1 mutant rescued mature endogenous miRNA expression less effectively than either WT hDcr or the smaller N1 mutant (Fig. 1 F and G). In subsequent experiments we therefore focused on the N1 hDcr truncation mutant. It should be noted that transfection of NoDice cells with hDcr expression plasmids results in a significant, ~20-fold higher level of hDcr expression than seen in the parental 293T cells (Fig. S1C). Therefore, subsequent functional experiments are actually looking at phenotypes that reflect hDcr overexpression.

Because it has been suggested that deletion of the amino-terminal helicase domain of hDcr can unmask a normally cryptic nuclear localization signal, resulting in the nuclear localization of the normally exclusively cytoplasmic hDcr protein (18), we also analyzed the subcellular localization of the WT and N1 variants of hDcr by immunofluorescence using a polyclonal anti-Dicer antiserum. As shown in Fig. S2, we observed that the WT and N1 hDcr mutant both remained restricted to the cytoplasm in expressing NoDice cells.

Human Dicer Can Process Long dsRNAs to Generate Functional siRNAs.
A key question was whether the N1 mutant of hDcr would be able to process long, perfect dsRNAs into functional siRNAs. For this purpose, we constructed a plasmid, termed pCD-RLuc, containing two Pol III-dependent promoters that convergently
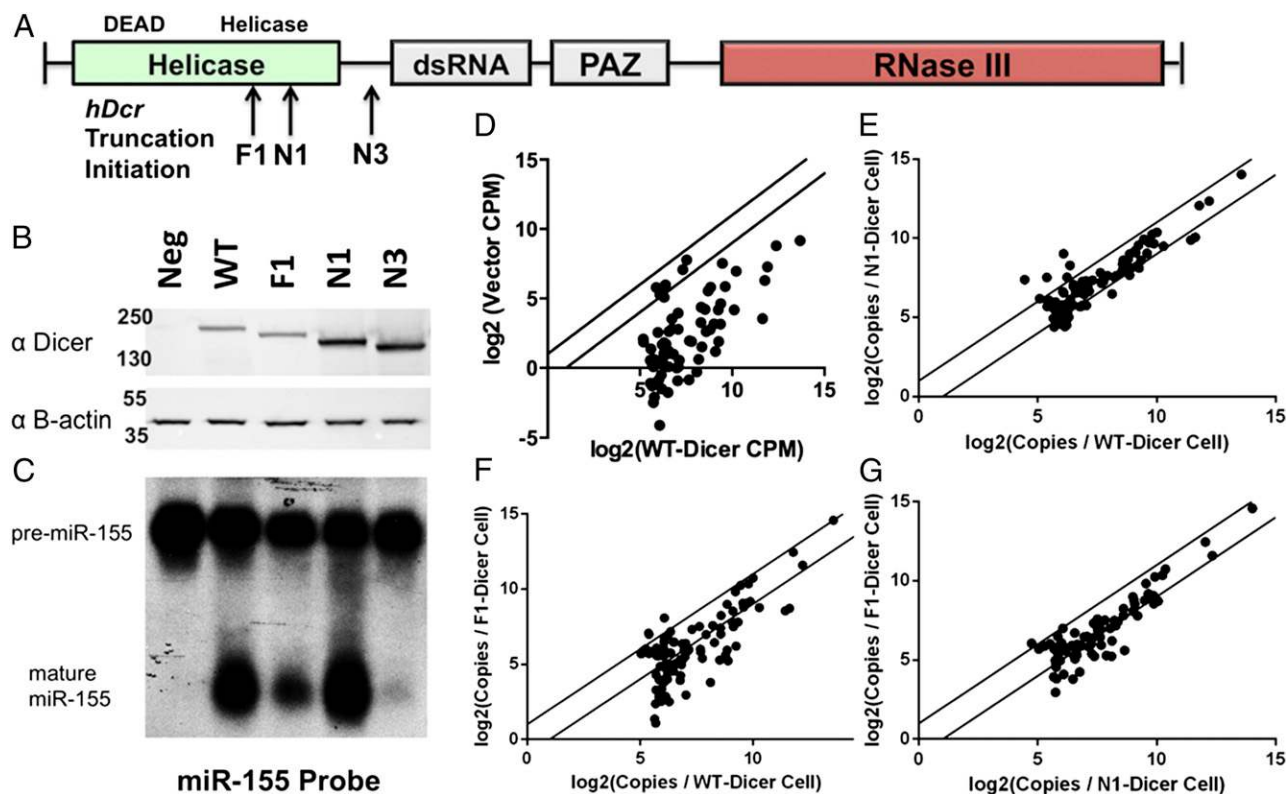

Fig. 1. Generation of functional truncations of the hDcr helicase domain. (*A*) Three N-terminal truncation mutants of the hDcr helicase domain were generated. F1 was generated as described previously (13), and N1 and N3 were designed to remove the N-terminal DEAD box or the entire helicase domain, respectively. Expression analyses were performed in the NoDice cell line, which is Dicer-null (17). (*B*) Expression of hDcr proteins detected by Western blot of transfected NoDice cell extracts probed with a polyclonal Dicer antiserum. (*C*) Capacity for pre-miRNA processing was analyzed by Northern blot. The upper band represents pre-miR-155, whereas the lower band corresponds to mature miR-155. (Probe specificity is further confirmed in Fig. S1A). (*D–G*) Mature miRNA expression, determined by small RNA-seq. *D* shows data normalized to the entire read yield because of the almost complete lack of mature miRNAs in the vector transfected NoDice cells, and is given in counts per million (cpm). In contrast, the data shown in *E–G* are normalized to the total number of miRNAs per cell.

transcribe opposite strands of a 257-bp gene segment derived from the *Renilla* luciferase (RLuc) gene. Not unexpectedly, transfection of NoDice cells with this plasmid produced an acute cytopathic effect, which we hypothesized likely primarily arose because of induction of the host innate-immune factor protein kinase RNA-activated (PKR), which is activated by binding to long dsRNAs and then blocks mRNA translation (19, 20). Therefore, we further modified the NoDice cells by using the bacterial CRISPR/Cas DNA editing machinery (21) to inactivate all three copies of the human *pkr* gene. As shown in Fig. 2*A*, the resultant NoDice/ΔPKR cells express neither hDcr nor PKR. Moreover, transfection of the NoDice/ΔPKR cells with the pCD-

RLuc plasmid no longer induced the acute cytotoxicity seen in 293T or NoDice cells.

The availability of the NoDice/ΔPKR cell line allowed us to test whether the 257-bp dsRNA expressed by pCD-RLuc could be processed into siRNAs by either WT or N1 hDcr. For this purpose, NoDice/ΔPKR cells were cotransfected with pCD-RLuc and an empty vector, or vectors expressing WT or N1 hDcr. Small RNA transcripts (<200 nt) were then harvested at 48 h posttransfection and subjected to small RNA-seq, as previously described (17), and the data analyzed for the origin of the reads obtained (Table S1). In the control transfected NoDice/ΔPKR cells, short RNA reads (15–50 nt in length) derived from the predicted dsRNA insert
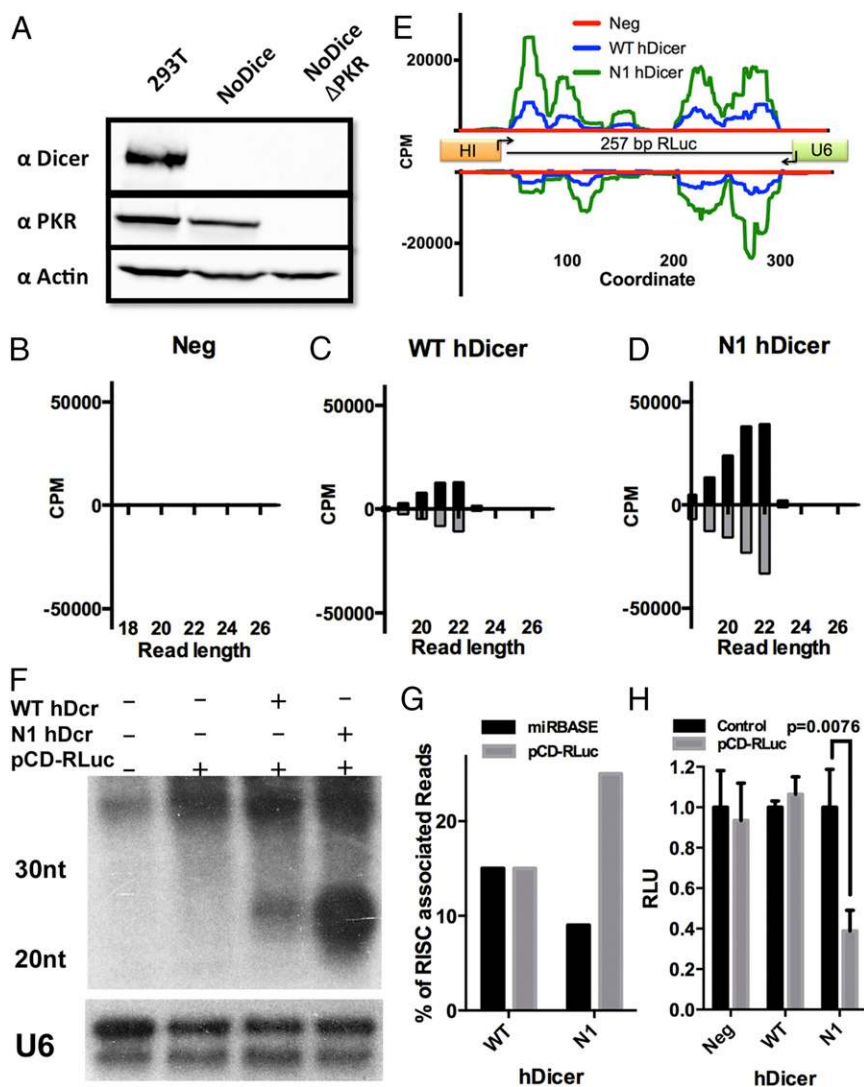

Fig. 2. Helicase-deficient hDcr can generate functional siRNAs from long dsRNAs. (*A*) To minimize the cytotoxic effects caused by expression of long dsRNAs in human somatic cells, we inactivated the *pkr* gene in NoDice cells by gene editing. This Western blot demonstrates that NoDice/ΔPKR cells are both hDcr and PKR deficient. (*B–D*) NoDice/ΔPKR cells were cotransfected with a dual Pol III dsRNA expression construct, consisting of a 257-bp fragment of RLuc flanked 5′ by an H1 and 3′ by a U6 promoter, together with an empty expression vector (Neg) or vectors expressing WT or N1 hDcr. Small RNA reads, 18–27 nt in length, derived from the predicted dsRNA were identified by small RNA-seq and are shown by read length distribution, normalized to the total number of reads obtained, and are given in counts per million. (*E*) The origin of small RNA reads 22 ± 2 nt in length, with duplex partners forming a 2-nt 3′ overhang, are shown for the entire duplex region present in pCD-RLuc. (*F*) Northern analysis of NoDice/ΔPKR cells transfected as indicated at the top of the panel using a probe specific for the dsRNA insert present in pCD-RLuc. Endogenous U6 was used as a loading control. (*G*) RISC-associated small RNAs were recovered from NoDice/ΔPKR cells cotransfected with pCD-RLuc and a WT or N1 hDcr expression plasmid by immunoprecipitation using a pan-Ago antiserum and subjected to small RNA deep sequencing. Reads that aligned to known mature human miRNAs or to the pCD-RLuc dsRNA insert were then computationally identified and are given here as a percentage of the total number of reads obtained. (*H*) Dual luciferase assays were performed with the indicator vector psiCheck2, which encodes RLuc and FLuc (the dsRNA expression vector targets RLuc). Assays were conducted as independent quadruplicates with technical triplicates and normalized to the FLuc internal control. RLuc activity is given in relative light units (RLU). Average of three independent experiments with SD and significance indicated.

represented 0.25% of the reads obtained. This increased to 7.04% in cells expressing WT hDcr and to a remarkable 23.9% of all short RNA reads in the NoDice/ΔPKR cells expressing the hDcr N1 mutant (Table S1). As shown in Fig. 2B, we did not recover a significant number of small RNAs of RLuc origin (18–26 nt in length) from NoDice/ΔPKR cells cotransfected with pCD-RLuc and the empty vector. In cells cotransfected with the WT hDcr expression plasmid, we observed a number of reads with the characteristics expected of siRNAs. Specifically, these reads were ~22 nt in length and derived from both strands of the RLuc-derived 257-bp dsRNA (Fig. 2C). The small RNA-seq data obtained using NoDice/ΔPKR cells cotransfected with pCD-RLuc and the N1 expression plasmid showed a similar trend but differed in that the number of candidate siRNAs was substantially increased (Fig. 2D), while maintaining their origin from both strands of the predicted dsRNA. Interestingly, alignment of the reads observed in the WT or N1 Dicer-expressing cells that had potential duplex partners giving rise to two 2-nt 3′ overhangs, the predicted structure for a duplex siRNA intermediate (8), revealed evidence of phasing on the dsRNA (Fig. 2E), consistent with either processive or sequential exonucleolytic processing from both termini by both WT and N1 Dicer, although the latter clearly generated a far higher number of reads.

Next, we asked if the siRNAs produced from the dsRNA encoded by pCD-RLuc would be present at levels sufficient to be detected by Northern analysis. As shown in Fig. 2F, we were indeed able to readily detect ~22-nt siRNAs of RLuc origin in NoDice/ΔPKR cells cotransfected with pCD-RLuc and the N1 expression vector, whereas NoDice/ΔPKR cells expressing WT hDcr gave a weaker, but still detectable, signal (Fig. 2F). A key question was whether these pCD-RLuc–derived small RNAs were in fact loaded into RISC and therefore potentially functional. We therefore immunoprecipitated RISC using a pan-Ago antibody, as previously described (22), and then used deep sequencing to identify RISC-loaded small RNAs. As shown in Fig. 2G and Table S2, analysis of RISC-associated small RNAs in NoDice/ΔPKR cells expressing ectopic WT hDcr showed that ~16% of the reads were mature human miRNAs and an almost identical percentage were derived from the predicted dsRNA transcribed from pCD-RLuc. In contrast, in the NoDice/ΔPKR cells expressing N1 hDcr, ~9% of the reads obtained were mature human miRNAs, whereas ~26% were derived from the RLuc-specific dsRNA made by pCD-RLuc. Therefore, these data demonstrate that, although both WT and N1 hDcr variant can generate both mature miRNAs and siRNAs, the N1 mutant is clearly more efficient than WT hDcr at processing long dsRNA substrates.

An obvious question is whether the RISC-loaded siRNAs generated from the RLuc insert in pCD-RLuc are indeed functional: that is, able to specifically down-regulate RLuc expression. To test this hypothesis, we used the psiCheck2 plasmid, which contains two independent cassettes expressing RLuc and firefly luciferase (FLuc), the latter functioning as an internal control. NoDice/ΔPKR cells were initially transfected with pCD-RLuc plus either a WT or N1 hDcr expression plasmid, and then cotransfected 96 h later with psiCheck2. As shown in Fig. 2H, we observed a substantial decrease in RLuc expression in the cells coexpressing pCD-RLuc and N1 and this difference was highly statistically significant ($P < 0.008$). In contrast, we did not observe a significant inhibition of RLuc expression in the NoDice/ΔPKR cells cotransfected with pCD-RLuc and the WT Dicer expression plasmid. In total, these data therefore demonstrate the production of high levels of functional, RISC-loaded siRNAs in somatic human cells expressing the N1 mutant of hDcr and an endogenously transcribed dsRNA substrate. Interestingly, expression of high levels of at least partly nuclear dsRNA transcripts had no evident effect on the cytoplasmic localization of both WT and N1 hDcr (Fig. S2).

To extend these data, we next used a derivative of the previously described expression plasmid pHR3476 (23), which is transcribed to yield an ~1,460-nt capped, poly-adenylated RNA containing a 287-nt inverted repeat derived from the HIV-1 *envelope* (*env*) gene. This RNA is predicted to fold into a 287-bp stem flanked by a 5′ unstructured region of ~65 nt, a similarly unstructured ~162 nt 3′UTR, and a large ~659-nt loop region. As shown in Table S1 and Fig. 3 A–C, we observed the same general pattern of small RNA expression documented in Fig. 2, but with fewer reads derived from the predicted RNA stem. Specifically, deep sequencing of the small RNAs in NoDice cells expressing this structured RNA in the absence of ectopic hDcr gave very few reads (574) derived from the predicted RNA stem. However, in the WT hDcr-expressing cells, this number increased to 5,549 reads, whereas in the N1 expressing NoDice cells the number of reads derived from the stem increased further to 15,561, an increase of >30-fold (Table S1).

Analysis of size distribution and origin of the small RNAs present in the N1-expressing NoDice/ΔPKR cells identified several thousand ~21-nt small RNAs derived from both sides of the predicted stem (Fig. 3C), whereas WT hDcr produced substantially lower but detectable levels (Fig. 3B). The parental NoDice/ΔPKR cells, lacking any hDcr isoform, again produced very few small RNAs derived from this predicted RNA stem (Fig. 3A). Assignment of potentially duplex reads to locations along the predicted stem produced a different pattern with this Pol II-derived dsRNA stem than seen with the discrete, Pol III-derived dsRNA analyzed in Fig. 2. In particular, although we did observe some evidence of phasing, especially for N1, the major peaks of siRNA production were not near the ends of the dsRNA, as seen in Fig. 2E, but rather near the center, possibly consistent with some form of endonucleolytic cleavage (Fig. 3D).

Analysis of the potential of these putative siRNAs to repress mRNA function was again tested using the psiCheck2 indicator plasmid, in this case using a variant in which one copy of the *env* sequence present in the RNA stem in pHR3476 was inserted into the 3′UTR of RLuc. As shown in Fig. 3E, we again observed significant ($P < 0.001$) repression of RLuc expression in the N1-expressing NoDice/ΔPKR cells, whereas the WT hDcr-expressing cells did not demonstrate a detectable level of RLuc repression. These data again indicate that the N1 mutant of hDcr is giving rise to functional siRNAs, in this case derived from an internal dsRNA stem present in an mRNA-like transcript.

Analysis of the Ability of Human Dicer to Generate Viral siRNAs. As noted above, it is believed that RNAi originally evolved as an innate antiviral immune response and it continues to serve this purpose in plants and invertebrates (1, 2). We therefore next asked whether the N1 hDcr mutant could give rise to siRNAs of viral origin in infected cells. The first virus tested was the plus-stranded picornavirus poliovirus (PV), which has previously been reported to give rise to low but detectable levels of "viral small RNAs" (vsRNAs) in infected somatic human cells, although loss of Argonaute 2 (Ago2), the "slicer" protein for RNAi, was found to have no effect on PV replication (4).

In this experiment, we transfected NoDice cells with a control vector, or vectors expressing WT or N1 hDcr, then transiently selected for transfected cells by antibiotic resistance before infecting the cells with PV strain Sabin at a multiplicity of infection (MOI) of 10 at 96-h posttransfection. Sixteen hours later, we harvested total small RNAs and performed small RNA deep sequencing. As shown in Fig. 4A, we observed a significant number of vsRNAs, of 18–27 nt in length, in the PV-infected NoDice cells. However, these did not cluster at the predicted 22 ± 2-nt size predicted for Dicer products and likely represented random degradation products derived primarily from the more highly expressed PV RNA (+) strand. Expression of WT hDcr resulted in a slight increase in the number of viral reads 22 ± 2 nt in length (Fig. 4B), although this effect was subtle and seen predominantly with reads of (+) strand origin, possibly consistent
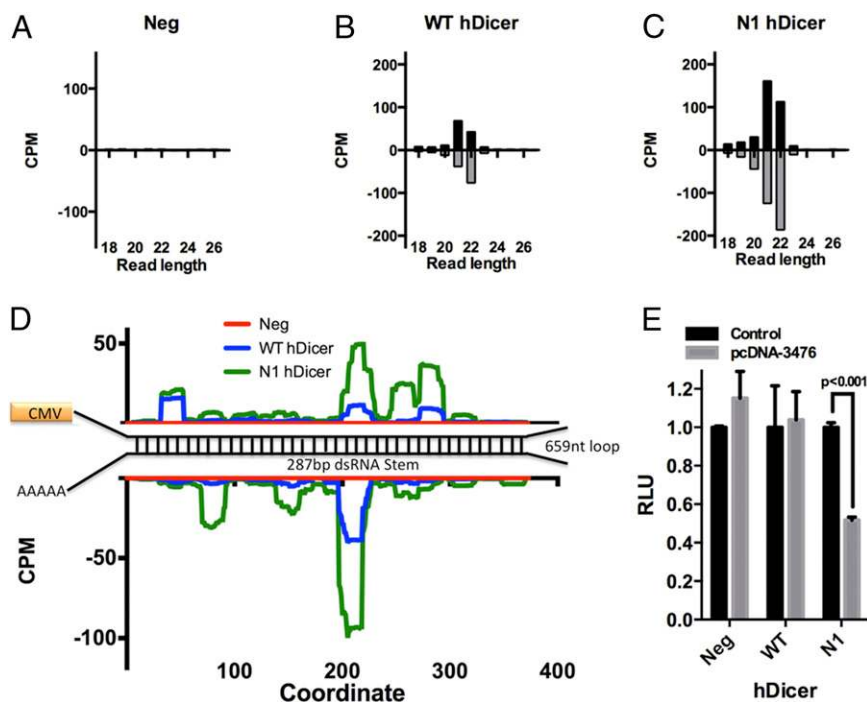
Fig. 3. The N1 hDcr mutant can generate functional siRNAs from a Pol II-transcribed RNA stem-loop. Similar to Fig. 2, these experiments were conducted in NoDice/ΔPKR cells by cotransfection followed by a similar downstream analysis. A previously described plasmid (23), which expresses a 287-bp RNA stem together with a large 659-nt terminal loop under the control of a Pol II promoter, was analyzed. NoDice/ΔPKR cells were cotransfected with this construct and an empty vector (Neg) or vectors expressing WT or N1 hDcr. At 48-h posttransfection, total RNA was harvested and small RNA-seq performed. (A–C) Read length distributions for reads derived from the stem of the predicted RNA stem-loop obtained by small RNA deep sequencing. (D) Small RNAs 22 ± 2 nt in length, with a duplex partner bearing a 2-nt 3′ overhang, were mapped onto the stem of the construct. (E) Dual luciferase indicator assays were performed with the 5′ arm of the stem inserted 3′ to the RLuc indicator gene in psiCheck2. Assays were conducted in quadruplicate with technical triplicates and were normalized to the FLuc internal control. The average RLuc activity in RLUs is shown with SD and significance indicated.

with a low level of processing by hDcr of RNA stem structures present on the PV (+) strand. In cells expressing N1 hDcr, the peak of RNA reads at 22 ± 2 nt in length was obvious (Fig. 4C) and, although this effect was again predominantly on (+) strand reads, a symmetrical peak of 22 ± 2-nt PV reads of (−) strand origin was nevertheless clearly present, thus suggesting that at least some of these reads result from N1 cleavage of viral dsRNA replication intermediates. However, unlike the experiments performed previously looking at siRNAs derived from endogenously transcribed dsRNAs, we did not observe an increase in the number of PV-derived small RNAs in the presence of the N1 hDcr mutant (Table S3), arguing that processing of PV-derived RNAs by N1 was inefficient. Analysis of the genomic origin of vsRNA reads predicted to be capable of forming siRNA duplexes showed that the PV-derived reads recovered from NoDice cells expressing N1 were concentrated at the 5′ end of the PV genome, in the highly structured internal ribosome entry site (IRES) (24), suggesting again that these reads at least partly resulted from N1-processing of viral stem structures (Fig. 4D). In contrast, very few predicted duplex PV reads were obtained from cells expressing WT Dicer, consistent with a previous report (4). We also observed a peak of vsRNA production from near the 3′ end of the PV genome, again primarily in the N1-expressing cells, which was derived equally from both the (+) and (−) strands of the PV genome, suggesting N1 cleavage of the PV dsRNA replication intermediate. A third peak, near coordinate 3050 of the PV genome, was detected equally in the presence and absence of hDcr and is of unknown origin (Fig. 4D).

Because we did not observe a significant inhibition of the level of PV replication in the presence of the N1 hDcr mutant, despite the increase in vsRNA reads in the presence of N1 (Fig. 4C), we next asked whether these small RNAs were in fact loaded into RISC. We therefore sequenced RISC-associated small RNAs in PV-infected NoDice cells expressing the WT or N1 form of hDcr, as previously described (22). Analysis of RISC-associated PV-derived reads (Fig. S3B) showed that some, but not all, of the PV-derived reads obtained from near the 5′ end of the PV RNA genome (Fig. 4D and Fig. S3A) were indeed loaded into RISC. In particular, we noted a major peak of RISC-loaded, PV-derived

small RNAs derived from a region ∼100 nt from the 5′ end of the PV genome in N1-expressing cells that was also barely detectable in the WT hDcr-expressing cells. Therefore, at least some PV-derived vsRNAs are indeed loaded into RISC. However, these reads appear to be almost entirely of (+) strand polarity, thus possibly explaining their weak inhibitory activity.

To extend this analysis, we next performed small RNA deep sequencing using RNA recovered from NoDice/ΔPKR cells expressing ectopic WT or N1 hDcr that had been infected with influenza A virus (IAV), a segmented negative-strand RNA virus. For this purpose, we infected NoDice cells overexpressing WT or N1 hDcr with IAV strain Puerto Rico/8/34 (PR8) at an MOI of 2.0. As shown in Fig. 5A, we recovered a substantial number of IAV-derived vsRNAs of 18–26 nt in length, of almost entirely (+) strand polarity, from IAV-infected NoDice/ΔPKR cells in the absence of ectopic hDcr and these did not cluster at any particular size. This pattern was only slightly changed in the NoDice/ΔPKR cells expressing ectopic WT hDcr, although we did detect an increase in the number of IAV-derived reads of 21 or 22 nt, particularly of minus sense polarity, that could represent siRNAs of IAV origin (Fig. 5B and Table S4). These potential siRNA reads were further increased in the IAV-infected NoDice/ΔPKR cells expressing ectopic N1 hDcr, where we observed an apparent peak of vsRNAs of 21–22 nt in size derived equally from the (+) and (−) strands of the IAV genome (Fig. 5C and Table S4). Further analysis showed that these vsRNAs derived primarily from the termini of the IAV genomic segments, as shown here by alignment of IAV small RNA reads of 22 ± 2 nt in length to the IAV PA, PB1, and PB2 genome segments (Fig. 5D). These data therefore suggest that the N1 hDcr mutant was able to process the termini of viral dsRNA replication intermediates to produce readily detectable levels of IAV-derived siRNAs.

To determine if these potential siRNAs might be able to affect IAV replication, we cotransfected NoDice/ΔPKR cells with either the control pK plasmid or pK derivatives encoding WT or N1 hDcr together with a plasmid encoding a blastocidin-resistance marker. After selection for blastocidin resistance, the cells were infected with IAV strain PR8 at an MOI of 1.0 or 0.1. At 24-h postinfection, the cells were harvested and the level of the IAV
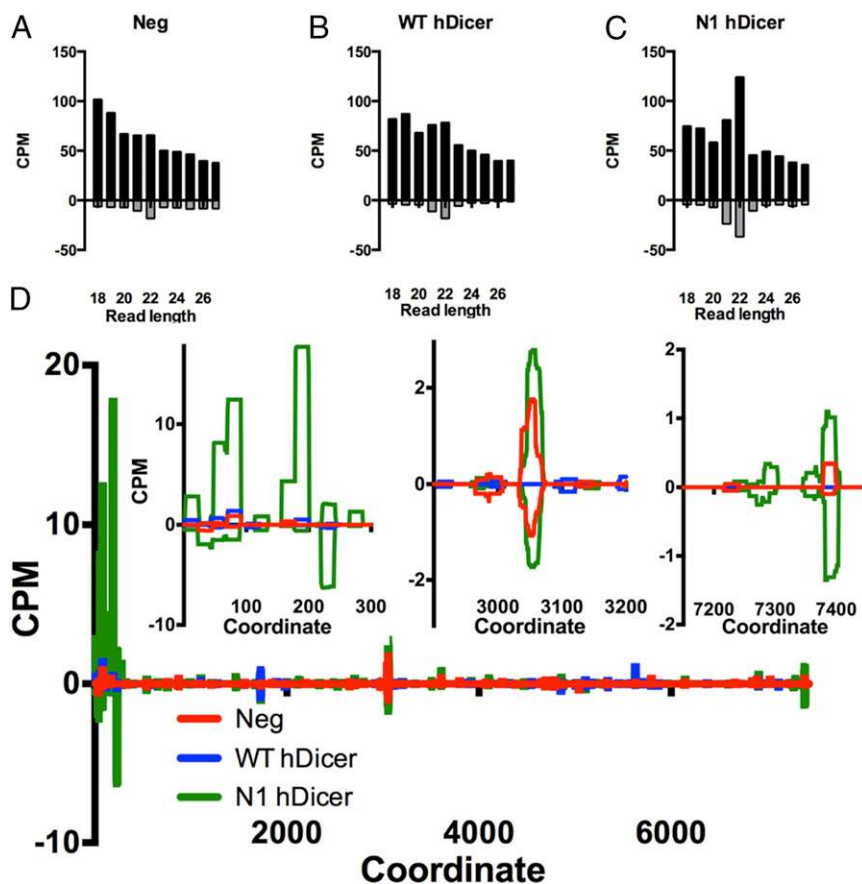
Fig. 4. N1 hDcr generates low levels of poliovirus-derived siRNAs in infected cells. NoDice cells were cotransfected with a blasticidin acetyltransferase expression vector together with a WT or N1 hDcr expression vector or a matched empty vector (Neg). The cells were then selected for blasticidin resistance and infected with PV for 16 h. (*A–C*) Small RNA read length distribution for reads aligning to the PV genome, normalized to the total number of small RNA reads obtained and given in counts per million. (*D*) RNA reads 22 ± 2 nt in length, potentially able to form a duplex with an antisense read to give a 2-nt 3′ overhang, are shown relative to the PV genome. The inlays depict in further detail the 5′ and 3′ termini of the PV genome (*Left* and *Right*), and a central location where short RNA reads were obtained under all conditions, including in the absence of hDcr (*Center*).

NP segment quantified by qRT-PCR. As shown in Fig. 5*E*, we observed a significant ($P < 0.001$) decline in the level of the IAV NP transcript in NoDice/ΔPKR cells infected with IAV at an MOI of 1.0 if these expressed the N1 hDcr mutant but no effect when WT hDcr was overexpressed. In the NoDice/ΔPKR culture infected in parallel at an MOI of 0.1, we saw a trend toward an inhibition in IAV NP transcript expression in the presence of the N1 hDcr mutant that was however not statistically significant ($P = 0.07$). In cells overexpressing WT hDcr, we again saw no change in NP RNA expression relative to NoDice/ΔPKR cells transfected with the control pK plasmid. We conclude that overexpression of the N1 hDcr mutant, but not of WT human hDcr, results in the production of a level of IAV-specific siRNAs that is sufficient to at least modestly reduce the replication of IAV in infected cells.

Overexpression of IAV-Encoded Proteins Can Inhibit siRNA Biogenesis. We next asked whether IAV had the ability to inhibit siRNA biogenesis or function. To test the latter hypothesis, we transfected NoDice/ΔPKR cells, as described in Fig. 2*H*, with pCD-RLuc and a control or N1 hDcr expression plasmid. After selection for blasticidin resistance, the NoDice/ΔPKR cells were replated and transfected with the psiCheck2-based reporter as described in Fig. 2*H*. An additional 24 h later, the NoDice/ΔPKR cells were infected with IAV at an MOI of 2.0 and the cells then lysed and analyzed for luciferase expression. As shown in Fig. S4, infection with IAV did not affect the observed inhibition of RLuc expression by siRNAs generated by N1 from the dsRNA transcript encoded by pCD-RLuc. This result is consistent with previous results demonstrating that IAV mutants bearing inserted miRNA target sites are highly susceptible to inhibition by the cognate cellular miRNA if it is present in infected cells (25).

Although it has previously been demonstrated that IAV can be engineered to express functional miRNAs in infected cells (26,

27), thus demonstrating that IAV infection does not block Dicer's ability to process short RNA hairpins, we were nevertheless interested in asking whether overexpression of the IAV NS1 or NP protein would result in a detectable inhibition of siRNA biogenesis from long dsRNAs. Indeed, it has been reported that NS1 is able to inhibit siRNA biogenesis when overexpressed in plants (28) and this activity has been mapped to the amino-terminal dsRNA binding domain of NS1 (29). Because the assay used to test for siRNA production and function from the pCD-RLuc plasmid takes 6 d (Fig. 2*H*), we were not able to ask whether IAV infection inhibited siRNA biogenesis as this results in cell death within 2 d. Instead, we asked whether ectopic expression of IAV NS1, or of IAV NP, another RNA binding protein, would inhibit siRNA biogenesis if these expression plasmids were cotransfected with the pCD-RLuc and N1 hDcr expression plasmids, as described in Fig. 2*H*. As shown in Fig. 6*A*, we observed a complete reversal of the repression of RLuc expression by the combination of pCD-RLuc and N1 hDcr when IAV NS1 was ectopically overexpressed and a partial reversal upon ectopic expression of IAV NP. This finding correlated with a significant reduction in the production of pCD-RLuc-derived siRNAs, as detected by Northern blot (Fig. 6*B*). Therefore, we can conclude that the ectopic overexpression of IAV NS1 and, to a lesser extent IAV NP, can inhibit the biogenesis of siRNAs (Fig. 6) but not the function of RISC-loaded siRNAs (Fig. S4).

Discussion

Efforts to demonstrate the production of functional siRNAs in mammalian somatic cells infected by viruses or transfected with dsRNA expression vectors have repeatedly proven unsuccessful (4–7). This was surprising, as virus infection of plants or invertebrates generates readily detectable levels of siRNAs that play
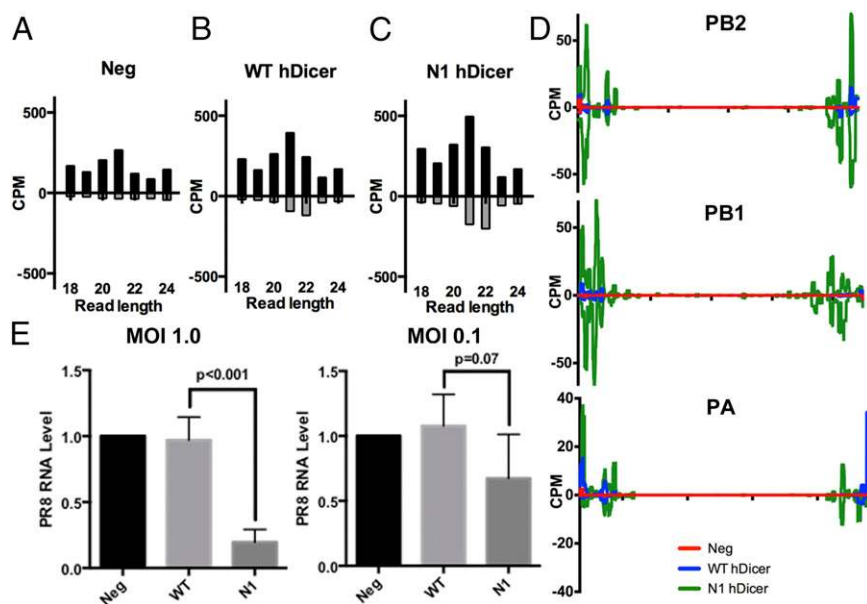
Fig. 5. Detection of viral siRNAs in IAV infected human cells. NoDice/ΔPKR cells were transfected and blasticidin-selected, as described in Fig. 4, and were then infected with IAV for 24 h at an MOI of 2.0. (*A–C*) Length distribution of small RNA reads aligning to the IAV genome, normalized to total read numbers given in counts per million, for cells lacking hDcr or expressing ectopic WT or N1 hDcr. (*D*) Coverage plots for IAV small RNA reads (22 ± 2 nt) aligning to IAV genome segments PB2, PB1, or PA and given in counts per million. (*E*) NoDice/ΔPKR cells expressing either the WT or N1 forms of hDcr were infected with IAV at the indicated MOI and total RNA harvested at 24-h postinfection. This bar graph depicts the expression level of IAV transcripts encoding the viral NP gene as determined by qRT-PCR. RNA levels were normalized to endogenous human β-actin mRNA and are given relative to the IAV NP RNA level detected in control vector-transfected NoDice/ΔPKR cells, which was set at 1.0. Average of three independent experiments with SD and significance indicated.

an important role in antiviral defense (1, 2). Moreover, although invertebrate animals can generate high levels of functional siRNAs from ectopically expressed or injected dsRNAs, mammalian somatic cells instead activate protein-based innate-immune responses that nonspecifically inhibit mRNA function and prevent the detection of gene-specific RNAi (30–32). However, dsRNAs appear able to induce a gene-specific RNAi response in mouse germ and ES cells (8–12, 32), and mouse oocytes have been reported to express a novel, N-terminally truncated isoform of Dicer not found in somatic cells (13). Importantly, germ cells and ES cells also lack many of the protein-based innate immune responses found in somatic cells (33, 34).

Four possible hypotheses for the lack of detection of siRNAs and dsRNA-induced RNAi in somatic mammalian cells, which are not mutually exclusive, can therefore be advanced.

First, especially in the case of ectopic dsRNA expression, the inability to detect functional siRNAs could be a result of the potent and nonspecific innate-immune responses that are trig-

gered in somatic mammalian cells by long dsRNAs and then globally inhibit mRNA function (30–32).

Second, the full-length Dicer isoform expressed in mammalian somatic cells might be intrinsically unable to process long dsRNAs into siRNAs, perhaps because of an inability to process dsRNAs whose ends are occluded by unstructured RNA sequences or by RNA modifications, such as a cap (13, 15, 16).

Third, in the case of viral infections, the low levels of siRNA production could be a result of the action of viral inhibitors of RNAi (35).

Fourth, viral dsRNA replication intermediates might be refractory to Dicer cleavage, perhaps because replication occurs in membrane-bound replication factories that Dicer cannot access (36, 37) or because the expression level of Dicer is too low to be able to cleave a significant number of viral dsRNAs.

In this report, we have attempted to test whether one or more of these hypotheses can explain the apparent lack of functional siRNAs in mammalian somatic cells. We were particularly interested in recent data suggesting that the N-terminal helicase
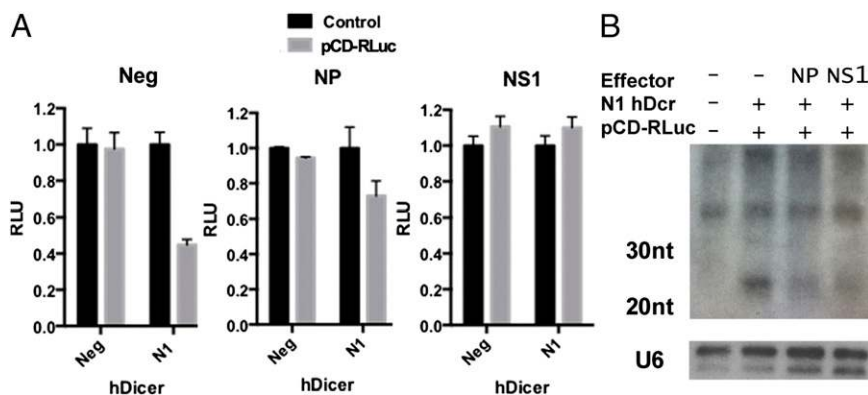

Fig. 6. The IAV NS1 and NP proteins can antagonize siRNA biogenesis. This experiment was designed to measure the ability of ectopically expressed IAV NS1 or NP to inhibit the production and function of siRNAs generated by the N1 hDcr mutant using the pCD-RLuc substrate, as described in Fig. 2. (*A*) Dual Luciferase indicator assays to measure the function of pCD-RLuc derived siRNAs generated by N1 hDcr were performed as described in Fig. 2*H*, except that the NoDice/ΔPKR cells were also cotransfected with vectors expressing IAV NS1 or NP, or with a similar RFP expression vector used as a negative (Neg) control. Average of three independent experiments with SD indicated. (*B*) Northern analysis of NoDice/ΔPKR cells cotransfected with pCD-RLuc, pK-N1 or the parental pK vector (negative control), and vectors encoding either the IAV NP or NS1 protein, using a probe specific for the dsRNA insert present in pCD-RLuc. Endogenous U6 RNA was used as a loading control.

domain of mammalian Dicer might act to selectively inhibit dsRNA but not pre-miRNA processing (13, 16). To this end, we generated several mutant forms of hDcr, lacking all or part of the helicase domain, and examined their ability to generate mature miRNAs when introduced into the previously described human NoDice cell line, which lacks a functional endogenous *dcr* gene (17). As shown in Fig. 1, we were able to identify a mutant form of hDcr, named N1, which lacks almost the entire helicase domain yet is fully competent for pre-miRNA processing.

Next, we asked whether overexpression of the full-length or N1 forms of hDcr would result in the processing of endogenously transcribed dsRNA substrates in human cells. The first substrate, transcribed by Pol III, was designed to have accessible dsRNA ends, whereas in the second substrate, transcribed by Pol II, the predicted dsRNA stem was flanked by unstructured RNA sequences, as well as by a cap and poly(A) tail. To avoid the issue of dsRNA-induced cytopathic effects, we generated a derivative of the NoDice cell line, NoDice/ΔPKR, where the *pkr* gene was also inactivated by DNA editing. These cells proved able to readily tolerate dsRNA expression and in the NoDice/ΔPKR cells transfected with the Pol III-dependent dsRNA expression vector, this allowed for the production of high levels of siRNAs that, in the N1 expressing cells, comprised ~24% of all small RNAs, as determined by small RNA-seq (Table S1) and that were efficiently loaded into RISC (Fig. 2*G*). Moreover, these small RNAs were of the correct, ~21-nt size (Fig. 2*D*), derived equally from both sides of the predicted dsRNA (Fig. 2*E*) and could be readily detected by Northern blot (Fig. 2*F*). Most importantly, these siRNAs proved able to selectively inhibit the expression of the cognate RLuc mRNA (Fig. 2*H*). To our knowledge, this is the first report documenting the production of a level of siRNAs in mammalian somatic cells that could not only be detected by the relatively insensitive Northern technique (Fig. 2*F*) but also give rise to the specific repression of the expected target mRNA (Fig. 2*H*). In the case of the internal dsRNA stem transcribed by Pol II, we also recovered readily detectable, but clearly lower, levels of siRNAs derived from a Pol II-transcribed internal RNA stem in the N1-expressing cells that were the correct, ~21-nt size (Fig. 3*C*), derived from both sides of the predicted dsRNA stem (Fig. 3*D*) and were again able to repress the expression of a cognate reporter plasmid (Fig. 3*E*).

Based on these data, it is clear that overexpression of the N1 hDcr mutant, which lacks almost the entire N-terminal helicase domain (Fig. 1), results in the efficient processing of dsRNAs with exposed termini to produce high levels of functional siRNAs (Fig. 2). When presented with an internal dsRNA stem, in an otherwise largely unstructured RNA transcript, the production of siRNAs appears to be less efficient (although we do not know the relative availability of these two dsRNA substrates). However, siRNAs were still readily detectable and were clearly functional (Fig. 3).

Although the hDcr N1 mutant is clearly more effective at dsRNA processing, we nevertheless also recovered siRNAs from cells expressing full-length hDcr, albeit at an ~fourfold lower level. Surprisingly, however, we were not able to show that these siRNA were functional (Figs. 2*H* and 3*E*). Although the reason for this lack of activity is unclear, it does not seem to be primarily because of the lower dsRNA processing efficiency of full-length hDcr, as this WT enzyme produced more siRNAs in the cells transfected with the Pol III-dependent dsRNA expression vector than did the N1 hDcr mutant in the cells transfected with the Pol II-dependent vector (compare Fig. 2*C* with Fig. 3*C*) and these were clearly loaded into RISC (Fig. 2*G*). Rather, we hypothesize that these functional data may underestimate the level of inhibition by RNAi because of the fact that NoDice cells transfected with either the WT or N1 hDcr expression plasmids divide considerably faster than the parental NoDice cells, and appear generally healthier, because of their reacquisition of endogenous miRNAs (Fig. 1) (17).

Although the data presented in Figs. 2 and 3 clearly demonstrate that at least the N1 mutant of hDcr is fully competent to generate functional siRNAs from dsRNA substrates, N1 proved unable to mount an effective RNAi response when expressed in cells infected by PV. In the PV-infected cells, the number of siRNAs obtained in WT hDcr expressing NoDice cells was negligible (Fig. 4*B*), and only improved slightly in NoDice cells expressing N1 (Fig. 4*C*). Moreover, the ~21-nt siRNAs that were obtained were largely derived from the IRES region of the PV RNA (+) strand (Fig. 4*D*) and, even though they were at least in part loaded into RISC (Fig. S3*B*), would therefore not be able to guide RISC to PV-derived mRNAs. This finding likely explains our inability to detect a significant level of inhibition of PV replication in NoDice cells in the presence of either WT of N1 hDcr and also a previous report that PV replicates normally in Ago2-deficient cells (4).

In contrast, in N1-expressing NoDice/ΔPKR cells infected by IAV, we observed a significantly higher production of ~22-nt RNAs of IAV origin and these derived from both the positive-sense (mRNA plus cRNA) and negative-sense (vRNA) transcripts generated by IAV during the replication cycle (Fig. 5*C*). Most importantly, these potential siRNAs derived predominantly from both ends of the IAV gene segments (Fig. 5*D*), consistent with their identity as potential siRNAs resulting from the exonucleolytic cleavage of IAV dsRNA replication intermediates by the N1 hDcr mutant. How hDcr, a cytoplasmic protein (Fig. S2), would gain access to these IAV dsRNA replication intermediates, which are thought to be generated exclusively in the cell nucleus, is however not clear.

Given that the N1 hDcr mutant appeared capable of generating a modest but readily detectable level of siRNAs of IAV origin, we next tested whether expression of N1 hDcr would be able to induce a significant inhibition in IAV replication as measured by qRT-PCR of viral transcripts. Indeed, as shown in Fig. 5*E*, we observed a significant ($P < 0.001$) reduction in IAV RNA expression in NoDice/ΔPKR cells infected with an MOI of 1.0 and a trend toward inhibition of IAV RNA expression when an MOI of 0.1 was tested ($P = 0.07$). Therefore, these data demonstrate that overexpression of the N1 hDcr mutant can exert a modest but significant inhibitory effect on IAV replication because of the production of IAV-specific siRNAs. As noted above, this contrasts with PV, where we observed low levels of siRNA production by N1 from almost exclusively the viral RNA (+) strand (Fig. 4), which did not result in a significant inhibition of PV replication. The mechanisms underlying this phenotypic difference are unknown, but one obvious possibility is that PV replicates so rapidly and induces cell death so quickly that the cell has insufficient time to accumulate a phenotypically relevant level of PV-derived siRNAs.

In a set of related experiments, we also asked whether the IAV NS1 protein, which has been previously reported to inhibit RNAi in plants (28, 29), could also exert this phenotype in human cells. Indeed, overexpression of IAV NS1, and to a lesser extent NP, inhibited both the production (Fig. 6*B*) and function (Fig. 6*A*) of siRNAs derived by N1 hDcr processing of the dsRNA insert encoded by the pCD-RLuc plasmid (Fig. 2). Therefore, it appears that NS1, which is known to avidly bind to dsRNAs (29, 38), is able to inhibit hDcr cleavage of long dsRNAs to generate RISC-loaded siRNAs in this experimental context. We note, however, that overexpression of the N1 hDcr mutant resulted in the production of IAV-derived siRNAs that induced a modest but significant inhibition of IAV replication (Fig. 5), thus clearly demonstrating that physiological levels of NS1 and NP do not fully block hDcr function. Moreover, it has been reported that IAV mutants engineered to express natural or artificial miRNAs can express these at readily detectable levels (26, 27), thus demonstrating that endogenous WT hDcr retains the ability to process premiRNA hairpins in IAV-infected cells. This finding suggests that the observed inhibition of siRNA production by NS1 and NP (Fig. 6) results from their overexpression in transfected

cells and suggests that long dsRNAs are a better substrate for NS1 or NP binding than are short pre-miRNA hairpins.

The aim of this manuscript was to test whether it is possible to induce the production of functional siRNAs in human somatic cells by manipulating different aspects of hDcr expression to shed light on why human somatic cells do not normally mount a protective RNAi response to viral infection. To this end, we have both substantially overexpressed WT and mutant hDcr variants (Fig. S1C) and tested truncation mutants of hDcr lacking the amino-terminal helicase domain (Fig. 1) that has been proposed to inhibit hDcr function in *cis* (13, 16). Moreover, these experiments were predominantly performed in cells engineered to lack functional copies of the endogenous *pkr* gene, to avoid artifacts caused by activation of endogenous immune responses as a result of dsRNA expression. Only in this rather artificial setting were we able to detect the production and function of siRNAs of both plasmid (Figs. 2 and 3) and viral (Fig. 5) origin, and even then we have only detected RNAi in cells overexpressing the N1 hDcr deletion mutant and not in cells overexpressing WT hDcr (Figs. 2, 3, and 5). Similarly, although we have confirmed previous data derived in plants showing that overexpression of the IAV NS1 protein can inhibit the production of siRNAs from long dsRNAs (28, 29), we note that this is, in fact, a general property of dsRNA binding proteins of even prokaryotic origin (39). Therefore, it will be necessary to conduct experiments using IAV mutants lacking a functional NS1 protein to determine unequivocally whether NS1-mediated repression of siRNA biogenesis from long dsRNAs occurs in IAV-infected, WT somatic cells and is phenotypically relevant. Previous data showing that IAV mutants lacking NS1 replicate and induce disease in mice that are deficient in IFN signaling, but not in WT mice (40), suggest that the known role of IAV NS1 in inhibiting the IFN response (41) is likely to be the only relevant activity of NS1 in WT cells.

In conclusion, to our knowledge this report demonstrates for the first time the production of readily detectable, functional siRNAs in human somatic cells. Our data also confirm previous reports arguing that the N-terminal helicase domain moderately inhibits dsRNA processing by hDcr (13, 16) and demonstrate that overexpression of hDcr mutants that lack this domain can result in the production of levels of siRNAs of viral origin that can modestly inhibit the replication of some (e.g., IAV) but not all (e.g., PV) RNA viruses. Whether RNAi can ever be an effective innate antiviral response in mammalian cells, including germ cells, therefore currently remains unclear.

Experimental Procedures

Molecular Clones. N-terminal hDcr truncations were designed around existing potential start codons in the hDcr coding sequence (CDS): N1 initiates at Met-496 and N3 initiates at Met-606. F1 was designed based on published work identifying a germ cell-specific murine Dicer isoform (13) and consists of a murine retroelement-derived 7-aa leader fused to the beginning of HDcr exon 7. All hDcr expression constructs (pK-N1, pK-N3, pK-F1, as well pK-WT) contain a N-terminal Flag epitope tag fused in frame and are expressed from the base vector pK (17), which was also used as a negative control (Neg).

Two constructs were designed to express long dsRNA templates for the purpose of reconstituting RNAi in human cells. First, a 257-bp fragment of the RLuc CDS was PCR-amplified and cloned into pSuper (Addgene) between two Pol III-dependent promoters, H1 and U6. This construct, named pCD-RLuc, therefore expresses two overlapping, convergent transcripts that can form a perfect 257-bp dsRNA bearing a 1-nt 3′ overhang at the 5′ end and an 8-nt 5′ overhang at the 3′ end. To test whether siRNAs can also arise from RNA stem-loop structures, we PCR-amplified a 1,233-bp insert, containing a 287-bp stem and a 659-nt loop derived from the HIV-1 *env* sequence present in pHR3476 (23) and cloned this into pcDNA3 to allow Pol II-mediated transcription of the inverted repeat (pcDNA-3476). The expression vectors encoding red fluorescent protein (RFP), IAV NS1, or IAV NP have been previously described (42).

Cell Culture. The 293T-derived NoDice(4-25) cell line, which is hDcr-deficient, has been previously described (17). 293T, NoDice, and NoDice/ΔPKR cells were cultured in Dulbecco's Modified Eagle Medium supplemented with 10% (vol/vol) FBS and Gentamicin (Gibco). An sgRNA sequence (5′-GAATA-

CATACCGTCAGAAGC-3′) targeting Exon1 of PKR was cloned into the Cas9 expression vector pX330 (Addgene #42230) as previously described (21). NoDice cells were plated in six-well plates at 50% confluency and then transfected with 4 μg of this PKR-specific Cas9/sgRNA expression construct. Cells were transfected a second time, single cell-cloned, and screened to identify an hDcr and PKR-deficient clonal cell line (NoDice/ΔPKR).

Functional Knockdown Assays with dsRNA Substrates. NoDice/ΔPKR cells were plated at 40% confluency in 10-cm² dishes and transfected with 5 μg of effector (pK, pK-WT, or pK-N1), 5 μg of the RNAi substrate (pCD-RLuc or pcDNA-3476) or a vector control (pSuper, pcDNA3), and 5 μg of a plasmid expressing the blasticidin acetyltransferase gene (pcDNA-Blast). Media was changed at 24 h posttransfection and Blast selection initiated 24 h later. Ninety-six hours posttransfection, the NoDice/ΔPKR cells were split into 12-well plates at 40% confluency and transfected with 10 ng of a psiCheck2-based reporter (Promega). Next, 500 ng of an hDcr and a dsRNA expression plasmid were cotransfected along with the reporters. Cells were lysed 48 h later and assayed using a Dual-Luciferase Reporter Assay Kit (Promega).

To determine whether IAV infection of NoDice/ΔPKR inhibited the siRNA biogenesis pathway (Fig. S4), the above experiment was repeated, except that transfected cells were infected with IAV strain PR8, at an MOI of 2.0, 24 h before harvest. Luciferase assays were then conducted as described above. To analyze the effect of IAV NS1 or NP expression on siRNA function, NoDice/ΔPKR cells were transfected with pCD-RLuc, an hDcr expression plasmid, and expression vectors encoding RFP, as a negative control, or the IAV NS1 or NP protein (42) at a ratio of 1:1:1, and then analyzed by luciferase assay as described above.

Western and Northern Blots. Expression of WT and mutant hDcr was verified using a rabbit polyclonal anti-Dicer antibody (Santa Cruz 30226). PKR was detected using a monoclonal antibody (Abcam ab32506). Northern blots for miR-155 were performed as previously described (17). Briefly, NoDice cells were cotransfected with a pri-miR-155 expression construct and probed with a ³²P-labeled oligonucleotide complementary to mature miR-155. For Northern analysis of siRNA production from the dsRNA substrate encoded by pCD-RLuc, NoDice/ΔPKR cells were cotransfected with pCD-RLuc and either pK, pK-WT or pK-N1. At 48-h posttransfection, cells were harvested and small RNAs isolated using a mirVana kit (Ambion). Equal RNA amounts (~10 μg) were separated by electrophoresis on a TBE-Urea gel, transferred to nylon membranes, cross-linked, and then incubated with a random primed probe generated from the pCD-RLuc insert (Roche, Random Primed DNA Labeling Kit). To analyze the effect of the IAV NS1 or NP proteins on siRNA biogenesis, the NoDice/ΔPKR cells were also cotransfected with expression vectors encoding either RFP, NS1, or NP (42).

Virus Infections. NoDice cells were seeded in 15-cm² dishes and cotransfected with the parental pK vector (Neg), pK-WT, or pK-N1 along with pcDNA-Blast. After 48 h, the cells were subjected to selection with blasticidin (10 μg/mL) for 48 h and then replated for infection in 15-cm dishes at 1.5×10^7 cells per dish. Infection with the PV Sabin strain was carried out at an MOI of 10 for 30 min to allow adsorption. Subsequently, the cells were washed and complete media added. At 16-h postinfection, when a virus-induced cytopathic effect was visible, adherent cells were harvested and total RNA isolated using TRIzol.

For all IAV strain PR8 infections, virus was diluted in media, added to the cells for 4 h, and then the supernatant was removed and replaced with fresh media. For deep sequencing of small RNAs in IAV-infected cells, NoDice/ΔPKR cells cultured in 10-cm² dishes were infected at an MOI of 2.0 and harvested 24-h postinfection with a mirVana small RNA kit. For qRT-PCR analysis of IAV replication in the presence and absence of hDcr, NoDice/ΔPKR cells were infected with IAV strain PR8 in six-well plates at an MOI of 0.1 or 1.0.

Small RNA Deep Sequencing. NoDice/ΔPKR cells were transfected with pK, pK-WT, or pK-N1 and a dsRNA expression vector at a ratio of 1:1 for 48 h, and these dishes were directly harvested and small RNAs (<200 nt) isolated using a mirVana kit (Ambion). For all other experiments, total RNA was isolated using TRIzol and small RNAs purified using the mirVana Kit. All small RNA input was then processed with the TruSeq Small RNA Sample Preparation Kit (Illumina). cDNA was generated as previously described (22). Briefly, adapter-ligated RNA was reverse-transcribed using SuperScript III (Life Technologies) and amplified using GoTaq green PCR master mix (Promega) with the TruSeq 3′ indices. DNA bands corresponding to ~145 bp were isolated by gel electrophoresis on 10% (wt/vol) polyacrylamide gels and sequenced on an Illumina HiSeq 2000. Sequencing of RISC-associated small RNAs was performed as previously described (22). RIP-seq was performed at 72-h posttransfection for the pCD-RLuc construct and 16-h postinfection with PV, as described above.

Deep Sequencing Analysis. Small RNA reads were analyzed as previously described (22). Initial reads were quality-filtered with Cassava 1.8.2. Reads >15 nt were collapsed into FASTA format with the FASTX-Toolkit (hannonlab.cshl.edu/fastx_toolkit/index.html) using the following pipeline: fastq_quality_filter –Q 33| fastq_to_fasta –Q 33 | fastx_clipper -a TruSeq-Index# -l 15 –c | fastx_collapser.

All reads were then subject to alignment using Bowtie v0.12.7 (43) with the following options: –a–best–strata –m 25. The reads were sequentially aligned and filtered to adapter sequences, miRBase v20 annotations of miRNA hairpins or mature miRNA sequences (44), Ensembl noncoding RNA database release 70 (45), human functional RNA database v3.4 (46), the vector or viral sequence of interest, and finally human genome 19. No mismatches were allowed for alignments to the different references, except the human genome, for which two mismatches were allowed. Human PV1 strain Sabin 1 (accession no. AY184219.1) was used for alignment as well as the reference sequence for pcDNA3. For IAV PR8 sequence analysis (segment accessions nos. EF1909790–EF190986) reads were aligned identically.

Bowtie alignments were further analyzed with in-house Perl scripts to calculate read size distributions per run. Duplex partner analysis was also completed with a Perl script that parses all reads in the size range of 20–24

and determines whether at least one read of opposite sense exists of identical size with 2-nt 3′ overhangs. Reads meeting these criterion were used to calculate coverage which was then normalized to reads per million based upon the run yield.

Quantitative RT- PCR Analysis. NoDice/ΔPKR cells were transfected with either pK, pK-N1, or pK-WT and then infected with IAV strain PR8 at an MOI of 1 or 0.1. Cells were harvested 24 h later and subjected to total RNA extraction using TRIzol. Total RNA was reverse-transcribed using a SuperScript III kit (Invitrogen) followed by SYBR green qPCR of cDNAs derived from the NP segment of PR8, normalized to a β-actin mRNA endogenous control. Primer sequences specific for the IAV PR8 NP segment were as follows: 5′-ACGGCTGGTCTGACTCACAT-3′ (forward) and 5′-TCCATTCCGGTGCGAA-CAAG-3′ (reverse). Data were analyzed using the ΔΔ Ct method (47).

1. Ding SW, Voinnet O (2007) Antiviral immunity directed by small RNAs. *Cell* 130(3):413–426.
2. Cullen BR, Cherry S, tenOever BR (2013) Is RNA interference a physiologically relevant innate antiviral immune response in mammals? *Cell Host Microbe* 14(4):374–378.
3. Fire A, et al. (1998) Potent and specific genetic interference by double-stranded RNA in *Caenorhabditis elegans*. *Nature* 391(6669):806–811.
4. Parameswaran P, et al. (2010) Six RNA viruses and forty-one hosts: Viral small RNAs and modulation of small RNA repertoires in vertebrate and invertebrate systems. *PLoS Pathog* 6(2):e1000764.
5. Backes S, et al. (2014) The Mammalian response to virus infection is independent of small RNA silencing. *Cell Reports* 8(1):114–125.
6. Bogerd HP, et al. (2014) Replication of many human viruses is refractory to inhibition by endogenous cellular microRNAs. *J Virol* 88(14):8065–8076.
7. Girardi E, Chane-Woon-Ming B, Messmer M, Kaukinen P, Pfeffer S (2013) Identification of RNase L-dependent, 3′-end-modified, viral small RNAs in Sindbis virus-infected mammalian cells. *MBio* 4(6):e00698-e13.
8. Maillard PV, et al. (2013) Antiviral RNA interference in mammalian cells. *Science* 342(6155):235–238.
9. Nejepinska J, et al. (2012) dsRNA expression in the mouse elicits RNAi in oocytes and low adenosine deamination in somatic cells. *Nucleic Acids Res* 40(1):399–413.
10. Babiarz JE, Ruby JG, Wang Y, Bartel DP, Blelloch R (2008) Mouse ES cells express endogenous shRNAs, siRNAs, and other Microprocessor-independent, Dicer-dependent small RNAs. *Genes Dev* 22(20):2773–2785.
11. Tam OH, et al. (2008) Pseudogene-derived small interfering RNAs regulate gene expression in mouse oocytes. *Nature* 453(7194):534–538.
12. Watanabe T, et al. (2008) Endogenous siRNAs from naturally formed dsRNAs regulate transcripts in mouse oocytes. *Nature* 453(7194):539–543.
13. Flemr M, et al. (2013) A retrotransposon-driven dicer isoform directs endogenous small interfering RNA production in mouse oocytes. *Cell* 155(4):807–816.
14. Provost P, et al. (2002) Ribonuclease activity and RNA binding of recombinant human Dicer. *EMBO J* 21(21):5864–5874.
15. Zhang H, Kolb FA, Brondani V, Billy E, Filipowicz W (2002) Human Dicer preferentially cleaves dsRNAs at their termini without a requirement for ATP. *EMBO J* 21(21):5875–5885.
16. Ma E, MacRae IJ, Kirsch JF, Doudna JA (2008) Autoinhibition of human dicer by its internal helicase domain. *J Mol Biol* 380(1):237–243.
17. Bogerd HP, Whisnant AW, Kennedy EM, Flores O, Cullen BR (2014) Derivation and characterization of Dicer- and microRNA-deficient human cells. *RNA* 20(6):923–937.
18. Doyle M, et al. (2013) The double-stranded RNA binding domain of human Dicer functions as a nuclear localization signal. *RNA* 19(9):1238–1252.
19. Munir M, Berg M (2013) The multiple faces of proteinkinase R in antiviral defense. *Virulence* 4(1):85–89.
20. Balachandran S, Barber GN (2007) PKR in innate immunity, cancer, and viral oncolysis. *Methods Mol Biol* 383:277–301.
21. Shalem O, et al. (2014) Genome-scale CRISPR-Cas9 knockout screening in human cells. *Science* 343(6166):84–87.
22. Flores O, Kennedy EM, Skalsky RL, Cullen BR (2014) Differential RISC association of endogenous human microRNAs predicts their inhibitory potential. *Nucleic Acids Res* 42(7):4629–4639.
23. Ward AM, Rekosh D, Hammarskjold ML (2009) Trafficking through the Rev/RRE pathway is essential for efficient inhibition of human immunodeficiency virus type 1 by an antisense RNA derived from the envelope gene. *J Virol* 83(2):940–952.
24. Balvay L, Soto Rifo R, Ricci EP, Decimo D, Ohlmann T (2009) Structural and functional diversity of viral IRESes. *Biochim Biophys Acta* 1789(9-10):542–557.
25. Perez JT, et al. (2009) MicroRNA-mediated species-specific attenuation of influenza A virus. *Nat Biotechnol* 27(6):572–576.
26. Varble A, et al. (2010) Engineered RNA viral synthesis of microRNAs. *Proc Natl Acad Sci USA* 107(25):11519–11524.
27. Schmid S, Zony LC, tenOever BR (2014) A versatile RNA vector for delivery of coding and noncoding RNAs. *J Virol* 88(4):2333–2336.
28. Delgadillo MO, Sáenz P, Salvador B, García JA, Simón-Mateo C (2004) Human influenza virus NS1 protein enhances viral pathogenicity and acts as an RNA silencing suppressor in plants. *J Gen Virol* 85(Pt 4):993–999.
29. Bucher E, Hemmes H, de Haan P, Goldbach R, Prins M (2004) The influenza A virus NS1 protein binds small interfering RNAs and suppresses RNA silencing in plants. *J Gen Virol* 85(Pt 4):983–991.
30. Paddison PJ, Caudy AA, Hannon GJ (2002) Stable suppression of gene expression by RNAi in mammalian cells. *Proc Natl Acad Sci USA* 99(3):1443–1448.
31. Caplen NJ, Fleenor J, Fire A, Morgan RA (2000) dsRNA-mediated gene silencing in cultured *Drosophila* cells: A tissue culture model for the analysis of RNA interference. *Gene* 252(1-2):95–105.
32. Yang S, Tutton S, Pierce E, Yoon K (2001) Specific double-stranded RNA interference in undifferentiated mouse embryonic stem cells. *Mol Cell Biol* 21(22):7807–7816.
33. Wang R, et al. (2013) Mouse embryonic stem cells are deficient in type I interferon expression in response to viral infections and double-stranded RNA. *J Biol Chem* 288(22):15926–15936.
34. Stein P, Zeng F, Pan H, Schultz RM (2005) Absence of non-specific effects of RNA interference triggered by long double-stranded RNA in mouse oocytes. *Dev Biol* 286(2):464–471.
35. Wu Q, Wang X, Ding SW (2010) Viral suppressors of RNA-based viral immunity: Host targets. *Cell Host Microbe* 8(1):12–15.
36. den Boon JA, Ahlquist P (2010) Organelle-like membrane compartmentalization of positive-strand RNA virus replication factories. *Annu Rev Microbiol* 64:241–256.
37. Netherton CL, Wileman T (2011) Virus factories, double membrane vesicles and viroplasm generated in animal cells. *Curr Opin Virol* 1(5):381–387.
38. Wang W, et al. (1999) RNA binding by the novel helical domain of the influenza virus NS1 protein requires its dimer structure and a small number of specific basic amino acids. *RNA* 5(2):195–205.
39. Lichner Z, Silhavy D, Burgyán J (2003) Double-stranded RNA-binding proteins could suppress RNA interference-mediated antiviral defences. *J Gen Virol* 84(Pt 4):975–980.
40. García-Sastre A, et al. (1998) Influenza A virus lacking the NS1 gene replicates in interferon-deficient systems. *Virology* 252(2):324–330.
41. Wolff T, Ludwig S (2009) Influenza viruses control the vertebrate type I interferon system: Factors, mechanisms, and consequences. *J Interferon Cytokine Res* 29(9):549–557.
42. Maamary J, et al. (2012) Attenuated influenza virus construct with enhanced hemagglutinin protein expression. *J Virol* 86(10):5782–5790.
43. Langmead B, Trapnell C, Pop M, Salzberg SL (2009) Ultrafast and memory-efficient alignment of short DNA sequences to the human genome. *Genome Biol* 10(3):R25.
44. Kozomara A, Griffiths-Jones S (2014) miRBase: Annotating high confidence microRNAs using deep sequencing data. *Nucleic Acids Res* 42(Database issue):D68–D73.
45. Flicek P, et al. (2014) Ensembl 2014. *Nucleic Acids Res* 42(Database issue):D749–D755.
46. Mituyama T, et al. (2009) The Functional RNA Database 3.0: Databases to support mining and annotation of functional RNAs. *Nucleic Acids Res* 37(Database issue):D89–D92.
47. Livak KJ, Schmittgen TD (2001) Analysis of relative gene expression data using real-time quantitative PCR and the 2(−Delta Delta C(T)) Method. *Methods* 25(4):402–408.